

Optical generation of direct current of Weyl exciton enhanced by surface plasmons

Ma Luo and Zhibing Li*

The State Key Laboratory of Optoelectronic Materials and Technologies
School of Physics
Sun Yat-Sen University, Guangzhou, 510275, P.R. China

We show that significant momentum transfer from optical laser wave to the Weyl excitons of a two-dimensional electron system is possible when the two-dimensional system is placed on a substrate that supports surface plasmons. The excitation transition amplitude of large momentum transfer is nonzero because the photon momentum is greatly enlarged by the surface plasmons. The electromagnetic mode of the laser is squeezed into the sub-wavelength region in the vicinity of the surface, that further enhances the excitation probability. We calculate the optically generated electric current of graphene on the substrate. The asymmetric distribution of the excited carriers leads to a direct electric current that depends on the incident angle of laser. The same configuration can be applied to directional excitation of other massless Dirac Fermions, such as surface states of topological insulators.

PACS numbers: 81.05.ue, 78.67.Wj, 73.22.Pr, 72.80.Vp

Photonic electron excitation obeys conservation of energy and momentum. In a low refraction index dielectric material, the photon momentum of an optical field is much smaller than that of the excited electron, thereby the photon momentum is usually neglected. We are interested in the situation that the refraction index is extremely high such that the momentum transfer in the optical excitation has important contribution. The extremely high refraction index material can be realized by the surface plasmons (SPs). Significant momentum transfer involved in the optical electron excitation leads to an optically driven electric current.

We consider graphene as an example. The low energy excitations of graphene having wave vectors near to two Dirac points, $\mathbf{K} = (\frac{4\pi}{3\sqrt{3}a}, 0)$ and $\mathbf{K}' = (-\frac{4\pi}{3\sqrt{3}a}, 0)$ in the (k_x, k_y) plane, are described by Weyl (massless Dirac) particles that have the linear dispersion, with $a = 0.142nm$ being the bond length between two neighbored carbon atoms. In the vicinity of \mathbf{K} for instance, $\varepsilon_{\mathbf{k}}^\lambda = \lambda\hbar v_F |\mathbf{k} - \mathbf{K}|$, with $\lambda = \pm 1$ for conduction band and valence band respectively, $v_F \approx c_0/330$ being the Fermi velocity, and c_0 being speed of light in the vacuum. [1, 2] Compared to the dispersion of photon in dielectric material with refraction index n and wave vector \mathbf{q} , $\hbar\omega = \hbar c|\mathbf{q}|/n$, it can be seen that for the same energy, the momentum of the electron is $330/n$ times larger than that of photon. For this reason, the previous investigation of optical excitation of graphene has neglected the wave vector of the optical field. [3, 4] This type of excitation is shown in Fig. 1(a) where the lower(upper) cone is the valence(conduction) band, the vertical blue lines with double arrows imply transitions with vanishing momentum transfer. Figures 1(b-d) illustrate the transitions with finite momentum transfer, which are obviously different from Fig. 1(a) by the rotation symmetry breaking

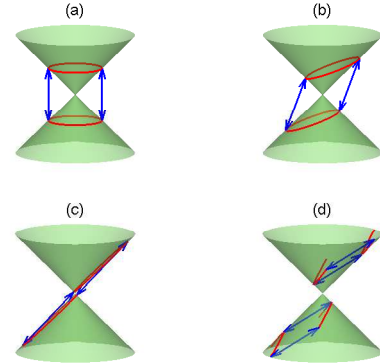


FIG. 1: The schematic picture for the optical transition in the Dirac cone of a 2D Weyl particle system, obeying energy and momentum conservation. In (a) the in-plane momentum of photon is zero. In (b), (c) and (d) the in-plane momentum of photon is non-zero, and phase velocity of the photon $\omega/|\mathbf{q}|$ is larger than, equal to, and smaller than that of the Weyl particle v_F , respectively.

that is the origin of the optical direct current.

The photon wavelength in dielectric is shortened by $1/n$, thereby the momentum of photon is enlarged by n . It is known that plasmonic systems consisting of a dielectric substrate with a plasmonic layer (doped graphene or metallic mono-atomic layer) imbedded in the vicinity of the surface can have effective refractive index of $n_{SP} \approx 300$. [5–7] The SPs propagate in the sub-wavelength region, with the squeezed E.M. field decaying at the out of plane direction exponentially. The plasmonic system strongly enhances the light-matter interaction because of highly localization of the optical field. [8] We consider a system in Fig. 2(a), where the plasmonic layer is imbedded in a dielectric substrate. The plasmonic layer can be modeled by Drude model of a 2D electronic gas. [9] In a practical setup, single mode SP

*Corresponding author: stslzb@mail.sysu.edu.cn

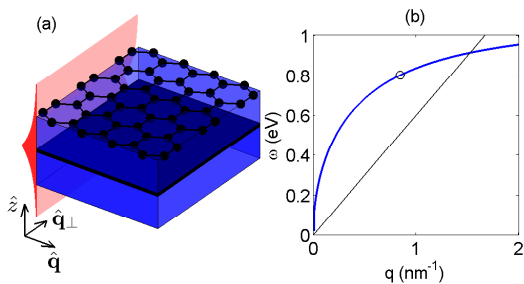


FIG. 2: (a) The schematic of the system with an imbedded plasmonic layer (black, consisted of doped graphene or metallic mono-atomic layer) and a graphene sheet on the top. The blue region is the dielectric substrate. The red part indicates the field profile of the SP mode, propagating along $\hat{\mathbf{q}}$ direction. (b) The typical dispersion of the SP mode of plasmonic layer (thick blue line) and the dispersion of the Weyl excitons of the graphene (thin black line). The circular point marks the SP mode that we choose for the numerical calculation.

of the plasmonic layer can be excited by optoacoustics method [10, 11]. The graphene that supports the optical current is on the top surface of the dielectric substrate, as shown in Fig. 2(a). The plasmonic layer is imbedded below the graphene of several decades of nanometers in depth such that the SP can interact with the graphene sheet.

The dispersion curve of the SP mode obtained by the semi-classical approximation is plotted in Fig. 2(b) as thick blue curve, which crosses the linear dispersion line of the Weyl particle (thin black line). A more accurate calculation using the random phase approximation [5, 6] gives a dispersion curve for the SP which is deviated from the thick blue curve at high energy region, and does not cross the straight line of the Weyl particle. For the SP mode with the energy of an optical photon, the wave number is of the same order of magnitude as that of the Weyl particle in graphene as shown in Fig. 2(b). Applying energy and momentum conservation, the allowed states excited by the E.M. field of the SP that propagates along $\hat{\mathbf{q}}$ are shown in Fig. 1(b) to (d) with red curves. For the SP mode with phase velocity $\omega/|\mathbf{q}|$ larger than v_F , the excitation process is shown in Fig. 1(b), which is an interband transition. Compared to the regular optical excitation of Fig. 1(a), the distributions of excited electron (the upper red circle) and hole (the lower red circle) is asymmetric in the 2D wave vector space. More forward electron states are excited than backward states, relative to the propagation direction of the SP mode. When the phase velocity of the SP mode approaches v_F , the allowed transitions are shown in Fig. 1(c). In this case, forward (backward) moving electrons (holes) are dominating. The phase volume of the states involved in the allowed transitions, which is the length of the red line in Fig. 1(c), has the same order of magnitude as that of regular optical excitation of Fig. 1(a). This is a specific property of massless Dirac fermion (Weyl particle) systems. For 2D non-relativistic electron gas, in contrast,

the dispersion is parabolic therefore the phase volume of the excited states shrinks to zero when the phase velocity of the SP mode decreases. For the SP mode with phase velocity smaller than v_F , only intraband transition is possible, as shown in Fig. 1(d) by the red curves. Because the valence band is fully filled for intrinsic graphene, this type of transition is negligible.

In our specific model, the plasmonic layer that support the SP mode consists of doped graphene with Fermi level being 0.66 eV (the black layer in Fig. 2(a)). The dielectric substrate is SiO_2 with permittivity being 1.5. The plasmonic layer is imbedded 20nm below the top surface. The separation between the graphene sheet on the top and the plasmonic layer is large enough such that their electronic states are uncoupled. The SP is localized near to the plasmonic layer with decay length around 6 nm. Thus, in the calculation of the dispersion of the SP mode, the boundary effect of the substrate can be neglected. We choose the SP mode with frequency being 0.8eV, which has a large momentum as well as a long propagation length. The phase velocity of this SP mode is larger than v_F , so that the optical transition corresponds to the case of Fig. 1(b). In order to have the optical transitions shown in Fig. 1(c) and (d), other 2D materials that support SP modes with smaller phase velocity is needed, and that is out of the scope of this article.

The electron in graphene is modeled by the tight binding theory, which gives the wave functions of the non-interacting eigenstates $|\lambda\mathbf{k}\rangle$ in real space as

$$\Psi_\lambda(\mathbf{k}, \mathbf{r}) = \sum_{s=A,B} C_\lambda^s(\mathbf{k}) \frac{1}{\sqrt{N}} \sum_{\mathbf{R}_s} e^{i\mathbf{k}\cdot\mathbf{R}_s} \phi(\mathbf{r} - \mathbf{R}_s) \quad (1)$$

with \mathbf{R}_s being the lattice vector of the A and B atoms, and $\phi(\mathbf{r} - \mathbf{R}_s)$ being the spatial wave function of the $2p_z$ orbital at lattice site \mathbf{R}_s . The energy level and coefficients C_λ^s are obtained by diagonalizing the Hamiltonian under the tight binding basis [1, 2].

The interaction Hamiltonian for Weyl particle in the field of the SP mode is,

$$H_I = -\frac{e_0}{m_0c} \mathbf{A} \cdot \mathbf{P} = i \frac{\hbar e_0}{m_0c} \mathbf{A} \cdot \nabla \quad (2)$$

where \mathbf{A} is the vector potential. Under the Coulomb gauge, $\mathbf{E} = -\frac{1}{c_0} \frac{\partial \mathbf{A}}{\partial t}$, with \mathbf{E} being the electric field of the SP mode. At the top surface, the in plane electric field of the SP mode at frequency ω , with in plane wave vector \mathbf{q} , is given by,

$$\mathbf{E}_{//} = \frac{E_0}{2} (e^{i\mathbf{q}\cdot\mathbf{r} - i\omega t} + e^{-i\mathbf{q}\cdot\mathbf{r} + i\omega t}) f(t) \hat{\mathbf{q}} \quad (3)$$

where $f(t)$ is a slowly varying envelope function, E_0 is the amplitude at the top surface, $\hat{\mathbf{q}}$ is the unit vector along the direction of \mathbf{q} . In our calculation, $E_0 = 1V/mm$ for the continue wave. The interaction between the electron and the \hat{z} component electric field of the SP mode is

neglected because of its small effect on the optical excitation of graphene. For a general SP wave package, such as Gaussian pulse, multiple modes with various \mathbf{q} should be included. In order to avoid the computational complexity, only SP of single mode will be considered. In the present work, the time profile function $f(t)$ is chosen to be the hyperbolic tangent function starting from zero, and with a turn-on time much larger than the period of the SP mode. Using the slow varying approximation that assumes $f'(t) \ll \omega$ and $Im[f(t)] = 0$, the interaction Hamiltonian is given as,

$$H_I = -i \frac{\hbar e_0}{m_0} \int_0^t \mathbf{E}(t') dt' \cdot \nabla \\ \approx \frac{\hbar e_0 E_0}{2m_0 \omega} f(t) (e^{i\mathbf{q}\cdot\mathbf{r}-i\omega t} - e^{-i\mathbf{q}\cdot\mathbf{r}+i\omega t}) \hat{\mathbf{q}} \cdot \nabla \quad (4)$$

Because of momentum conservation, the transition matrix elements are nonzero only if the initial and final Bloch wave vectors are different by $\pm\mathbf{q}$. Thus, the nonzero matrix elements of the SP absorption process are written as,

$$\langle \lambda' \mathbf{k} + \mathbf{q} | H_I | \lambda \mathbf{k} \rangle = \\ \frac{\hbar e_0 E_0 f(t)}{2m_0 \omega} \langle \lambda' \mathbf{k} + \mathbf{q} | e^{i\mathbf{q}\cdot\mathbf{r}} \hat{\mathbf{q}} \cdot \nabla | \lambda \mathbf{k} \rangle e^{-i\omega t} \quad (5)$$

with

$$\langle \lambda' \mathbf{k} + \mathbf{q} | e^{i\mathbf{q}\cdot\mathbf{r}} \hat{\mathbf{q}} \cdot \nabla | \lambda \mathbf{k} \rangle = \\ m \sum_{i=1}^3 \frac{\mathbf{b}_i \cdot \mathbf{q}}{|\mathbf{b}_i|} [C_{\lambda'}^{A*}(\mathbf{k} + \mathbf{q}) C_{\lambda}^B(\mathbf{k}) e^{i\mathbf{k}\cdot\mathbf{b}_i + \frac{1}{2}i\mathbf{q}\cdot\mathbf{b}_i}] \\ - m \sum_{i=1}^3 \frac{\mathbf{b}_i \cdot \mathbf{q}}{|\mathbf{b}_i|} [C_{\lambda'}^{B*}(\mathbf{k} + \mathbf{q}) C_{\lambda}^A(\mathbf{k}) e^{-i\mathbf{k}\cdot\mathbf{b}_i - \frac{1}{2}i\mathbf{q}\cdot\mathbf{b}_i}] \quad (6)$$

where \mathbf{b}_i ($i = 1, 2, 3$) are the three vectors from A atom to three nearest neighbored B atoms, $m \approx 3nm^{-1}$ is the norm of the matrix element of the Laplace operator between two nearest neighbored $2p_z$ orbitals. [12, 13] The matrix elements for the corresponding emission process are given by the complex conjugation of (5) and (6).

The interaction Hamiltonian couples eigenstates $|\lambda \mathbf{k}\rangle$ with eigenstates $|\lambda \mathbf{k} + \mathbf{q}\rangle$ for the SP absorption process, and with eigenstates $|\lambda \mathbf{k} - \mathbf{q}\rangle$ for the SP emission process. Define $\langle \lambda' \mathbf{k} | H_I | \lambda \mathbf{k} + \mathbf{q} \rangle = H_{\lambda' \mathbf{k}, \lambda \mathbf{k} + \mathbf{q}} f(t) e^{i\omega t}$ and $\langle \lambda' \mathbf{k} + \mathbf{q} | H_I | \lambda \mathbf{k} \rangle = H_{\lambda' \mathbf{k} + \mathbf{q}, \lambda \mathbf{k}} f(t) e^{-i\omega t}$. Applying the Heisenberg equation of motion, $i\hbar \partial_t \rho(t) = [\rho(t), H]$, under the basis of the non-interacting tight binding eigenstates, we obtain the Bloch equations of the density matrix. The time evolution equations of the diagonal terms are given as

$$\hbar \frac{\partial}{\partial t} \rho_{\lambda \mathbf{k}, \lambda \mathbf{k}} = -2Im[H_{\lambda \mathbf{k} + \mathbf{q}, \lambda \mathbf{k}} \rho_{\lambda \mathbf{k}, \lambda \mathbf{k} + \mathbf{q}} f(t) e^{-i\omega t}] \\ -2Im[H_{\bar{\lambda} \mathbf{k} + \mathbf{q}, \lambda \mathbf{k}} \rho_{\lambda \mathbf{k}, \bar{\lambda} \mathbf{k} + \mathbf{q}} f(t) e^{-i\omega t}] \\ +2Im[H_{\lambda \mathbf{k}, \lambda \mathbf{k} - \mathbf{q}} \rho_{\lambda \mathbf{k} - \mathbf{q}, \lambda \mathbf{k}} f(t) e^{-i\omega t}] \\ +2Im[H_{\lambda \mathbf{k}, \bar{\lambda} \mathbf{k} - \mathbf{q}} \rho_{\bar{\lambda} \mathbf{k} - \mathbf{q}, \lambda \mathbf{k}} f(t) e^{-i\omega t}] \quad (7)$$

where $\bar{\lambda} = -\lambda$ is the opposite band index. The time evolution equations of the microscopic polarization between interband eigenstates with the same Bloch wave vector are given as

$$\hbar \frac{\partial}{\partial t} \rho_{v \mathbf{k}, c \mathbf{k}} = i(\varepsilon_{c \mathbf{k}} - \varepsilon_{v \mathbf{k}}) \rho_{v \mathbf{k}, c \mathbf{k}} \\ - iH_{v \mathbf{k}, v \mathbf{k} + \mathbf{q}} \rho_{c \mathbf{k}, v \mathbf{k} + \mathbf{q}}^* f(t) e^{i\omega t} \\ + iH_{v \mathbf{k} + \mathbf{q}, c \mathbf{k}} \rho_{v \mathbf{k}, v \mathbf{k} + \mathbf{q}} f(t) e^{-i\omega t} \\ - iH_{v \mathbf{k}, c \mathbf{k} + \mathbf{q}} \rho_{c \mathbf{k}, c \mathbf{k} + \mathbf{q}}^* f(t) e^{i\omega t} \\ + iH_{c \mathbf{k} + \mathbf{q}, c \mathbf{k}} \rho_{v \mathbf{k}, c \mathbf{k} + \mathbf{q}} f(t) e^{-i\omega t} \\ + iH_{v \mathbf{k} - \mathbf{q}, c \mathbf{k}} \rho_{v \mathbf{k} - \mathbf{q}, v \mathbf{k}}^* f(t) e^{i\omega t} \\ - iH_{v \mathbf{k}, v \mathbf{k} - \mathbf{q}} \rho_{v \mathbf{k} - \mathbf{q}, c \mathbf{k}} f(t) e^{-i\omega t} \\ + iH_{c \mathbf{k} - \mathbf{q}, c \mathbf{k}} \rho_{c \mathbf{k} - \mathbf{q}, v \mathbf{k}}^* f(t) e^{i\omega t} \\ - iH_{v \mathbf{k}, c \mathbf{k} - \mathbf{q}} \rho_{c \mathbf{k} - \mathbf{q}, c \mathbf{k}} f(t) e^{-i\omega t} \quad (8)$$

The time evolution equations of the microscopic polarization between two eigenstates with Bloch wave vectors being different by \mathbf{q} are given as

$$\hbar \frac{\partial}{\partial t} \rho_{\lambda \mathbf{k}, \sigma \lambda \mathbf{k} + \mathbf{q}} = i(\varepsilon_{\sigma \lambda \mathbf{k} + \mathbf{q}} - \varepsilon_{\lambda \mathbf{k}}) \rho_{\lambda \mathbf{k}, \sigma \lambda \mathbf{k} + \mathbf{q}} \\ + iH_{\lambda \mathbf{k}, \sigma \lambda \mathbf{k} + \mathbf{q}} (\rho_{\lambda \mathbf{k}, \lambda \mathbf{k}} - \rho_{\sigma \lambda \mathbf{k} + \mathbf{q}, \lambda \mathbf{k} + \mathbf{q}}) f(t) e^{i\omega t} \\ + iH_{\bar{\lambda} \mathbf{k}, \lambda \mathbf{k} + \mathbf{q}} \rho_{\lambda \mathbf{k}, \bar{\lambda} \mathbf{k}} f(t) e^{i\omega t} \\ - iH_{\lambda \mathbf{k}, \sigma \bar{\lambda} \mathbf{k} + \mathbf{q}} \rho_{\sigma \bar{\lambda} \mathbf{k} + \mathbf{q}, \sigma \lambda \mathbf{k} + \mathbf{q}} f(t) e^{i\omega t} \quad (9)$$

with $\sigma = +$ and $\sigma = -$ for intraband polarization and interband polarizations respectively. This set of equations is the generalized optical Bloch equations.

Beside the optical excitation, the Coulomb scattering and phonon scattering will redistribute the excited electrons and holes. [12] We apply the relaxation time approximation for the scattering processes, so that the Bloch equation of each density matrix element has an additional decay term, $-\Gamma_{\lambda \mathbf{k}, \lambda' \mathbf{k}'} (\rho_{\lambda \mathbf{k}, \lambda' \mathbf{k}'} - \rho_{\lambda \mathbf{k}, \lambda' \mathbf{k}'}^0)$, whence the scattering processes are accounted. The scattering rate $\Gamma_{\lambda \mathbf{k}, \lambda' \mathbf{k}'}$ is approximated as constant Γ , and the scattering time is assumed to be $\hbar/\Gamma \approx 30fs$. The initial state is in equilibrium whose density matrix has vanishing off-diagonal elements and diagonal elements following the Fermi-Dirac distribution at the room temperature. The temperature is assumed unchanged in the following time. We are interested in the time regime much larger than the scattering time. The Bloch equations with the scattering terms are solved numerically for the time-depending density matrix to the time regime that the diagonal elements become stable and the off-diagonal elements exhibit periodic behavior. The resulted population of the excited electrons is shown in Fig. 3, which is the difference between the stable population under the continue wave excitation and the initial equilibrium population, i.e. $\rho_{c \mathbf{k}, c \mathbf{k}} - \rho_{c \mathbf{k}, c \mathbf{k}}^0$. The directional excitation is exhibited in the excited population of the electrons near K and K' points, which is consist with the theoretical

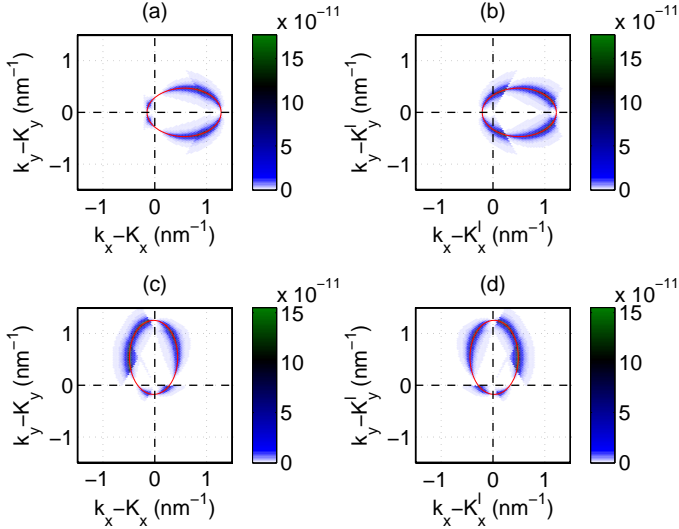


FIG. 3: (a) and (b) are population of excited electrons in conduction band near K and K' point, with the SP mode propagating along x axis or $\hat{q} = \hat{x}$. (c) and (d) are similar plots, with the SP mode propagating along y axis or $\hat{q} = \hat{y}$. The red curves indicate the theoretical selection rule of the optical excitation by the SP mode.

selection rules (red curves in Fig. 1) of energy and momentum conservation. However, not all of the selected states are excited equally because the transition amplitudes depend on the states and the propagation direction of the SP mode. The population of holes has similar distribution pattern as that of electron, with a translation of $-\mathbf{q}$ in the reciprocal space.

The current density can be calculated by the expectation value of the momentum operator as

$$\mathbf{j}(t) = \frac{e_0}{2Vm_0} \sum_{\lambda, \lambda', \mathbf{k}, \mathbf{k}'} \langle \lambda \mathbf{k} | \mathbf{p} - e_0 \mathbf{A}(t) | \lambda' \mathbf{k}' \rangle \rho_{\lambda \mathbf{k}, \lambda' \mathbf{k}'} + c.c. \quad (10)$$

Inserting the noninteracting basis functions of the tight binding theory (1), we obtain the formula for the total current as

$$\begin{aligned} \mathbf{j}(t) = & \frac{2\hbar e_0}{Vm_0} \left\{ 2 \sum_{\mathbf{k}} \text{Im}[\mathbf{M}^{vc}(\mathbf{k}) \rho_{v\mathbf{k}, c\mathbf{k}}] \right. \\ & - i \sum_{\mathbf{k}} [\mathbf{M}^{vv}(\mathbf{k}) \rho_{v\mathbf{k}, v\mathbf{k}} + \mathbf{M}^{cc}(\mathbf{k}) \rho_{c\mathbf{k}, c\mathbf{k}}] \\ & \left. - \frac{2e_0^2 E_0 c}{Vm_0 \omega} \hat{\mathbf{q}} \text{Im} \left[\sum_{\lambda, \lambda', \mathbf{k}} F_{\lambda' \mathbf{k} + \mathbf{q}, \lambda \mathbf{k}} \rho_{\lambda \mathbf{k}, \lambda' \mathbf{k} + \mathbf{q}}^* f(t) e^{-i\omega t} \right] \right\} \quad (11) \end{aligned}$$

where $\mathbf{M}^{\lambda \lambda'}(\mathbf{k}) = \langle \lambda \mathbf{k} | \nabla | \lambda' \mathbf{k} \rangle$ is the in-plane-momentum conserving optical transition matrix and $F_{\lambda' \mathbf{k} + \mathbf{q}, \lambda \mathbf{k}} = \langle \lambda' \mathbf{k} + \mathbf{q} | e^{i\mathbf{q} \cdot \mathbf{r}} | \lambda \mathbf{k} \rangle$. The component of the current associated with \mathbf{M}^{vc} is the interband current, and the components associated with \mathbf{M}^{vv} and \mathbf{M}^{cc} are the intraband currents. The current component that is directly proportional to E_0 is a pure alternative current. Because

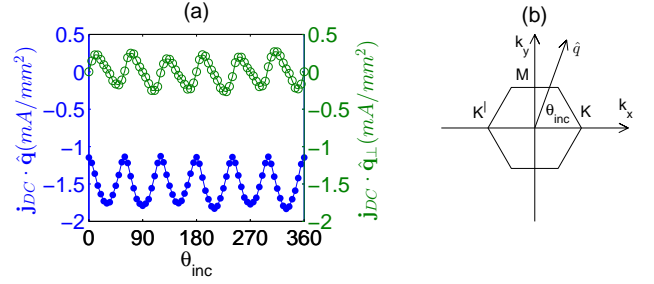


FIG. 4: (a) The DC component of the optically excited current along (perpendicular) to the propagation direction of the SP mode(or \hat{q}) shown as solid (empty) circles, versus the propagation angle of the SP mode(the angle from \hat{x} to \hat{q}). (b) indicates the direction of \hat{q} , and the K , K' and M points in the reciprocal space.

the SP excited population and polarization are not symmetric, both the interband and intraband currents are directional. For comparison, electrons and holes excited by the optical mode without the SP induced in-plane momentum transfer have centrosymmetric distributions in the reciprocal space. Therefore, there is no direct current in both conduction and valence bands.

Numerical result shows that the current contains a DC component, \mathbf{j}_{DC} , which can be extracted by fitting the stable solution of current with a horizontal line. \mathbf{j}_{DC} contains components along and perpendicular to the propagation direction of the SP mode(denoted by \hat{q} as shown in Fig. 4(b)). These two components of \mathbf{j}_{DC} are depending on the propagation angle of the SP mode, θ_{inc} , defined as the angle from \hat{x} to \hat{q} as shown in Fig. 4(a). The asymmetric population of carriers generates net forward(backward) flux of electrons(holes), so that the direct current along \hat{q} is negative. The direct current is symmetric under the rotation of \hat{q} by 60° because the hexagonal of the graphene is six-fold rotational symmetric. The magnitude of the direct current along \hat{q} minimize(maximize) when \hat{q} directs to one of the Dirac points (M points) because fewer(more) forward carriers are excited as observed in Fig. 3(a) and (b) ((c) and (d)). When \hat{q} directs to one of the Dirac points or M points the perpendicular component of the direct current is zero because the populations of the carriers have reflection symmetric to \hat{q} axis in reciprocal space.

In conclusion, the nano-structure consisting of a mono-atomic plasmonic layer imbedded in the vicinity of the surface of a dielectric substrate and a graphene sheet attached on the surface is designed for optical generation of direct electronic current in the graphene sheet. Origins for the direct electric current are: (1) the mono-atomic plasmonic layer squeezes the optical field in the surface region thus strongly enhances the light-matter interaction;(2) the mono-atomic plasmonic layer supports the SP mode that induces large momentum transfer in the optical excitations; (3) the excited particles and holes have asymmetric distribution in reciprocal space; (4) the

phase volume of the transitions of given energy and momentum remains finite due to the linear dispersion of the Weyl particles. We obtained the asymmetric distributions of the carriers by solving the Bloch equations of density matrix with the scattering term. The directional excitation of particles and holes opens a new way to generate direct current by optical means. It would be interesting to investigate the effect of surface plasmons on the optical directional excitation of the surface states of topological insulators [14], which also have Dirac cone dispersion.

Acknowledgments

We thank H.J. Kreuzer for valuable comments. The project is supported by the National Natural Sci-

ence Foundation of China (Grant: 11274393), the National Basic Research Program of China (Grant: 2013CB933601), and the National Key Research and Development Project of China (Grant: 2016YFA0202001).

References

-
- [1] A. H. Castro Neto, F. Guinea, N. M. R. Peres, K. S. Novoselov, and A. K. Geim, *Rev. Mod. Phys.*, **81**, 109(2009).
 - [2] D. N. Basov, M. M. Fogler, A. Lanzara, Feng Wang, and Yuanbo Zhang, *Rev. Mod. Phys.* **86** 959 (2014).
 - [3] Hamed Koochaki Keldar, Vadym Apalkov, and Mark I. Stockman, *Phys. Rev. B* **91**, 045439(2015).
 - [4] Anshuman Kumar, Andrei Nemilentsau, Kin Hung Fung, George Hanson, Nicholas X. Fang, and Tony Low, *Phys. Rev. B* **93**, 041413(R)(2016).
 - [5] M. Jablan, M. Soljacic, and H. Buljan, *Proceedings of the IEEE*, **101**, 1689(2013).
 - [6] M. Jablan, H. Buljan, and M. Soljacic, *Phys. Rev. B.*, **80**, 245435(2009).
 - [7] Z. Yuan, Y. Jiang, Y. Gao, M. Kaell, and S. Gao, *Phys. Rev. B* **83**, 165452(2011).
 - [8] Frank H. L. Koppens, Darrick E. Chang, and F. Javier Garcia de Abajo, *Nano Lett.* **11**, 3370(2011).
 - [9] E. H. Hwang and S. Das Sarma, *Phys. Rev. B* **75**, 205418(2007).
 - [10] Mohamed Farhat, Sebastien Guenneau, and Hakan Bagci, *Phys. Rev. Lett.* **111**, 237404(2013).
 - [11] Jurgen Schiefele, Jorge Pedros, Fernando Sols, Fernando Calle, and Francisco Guinea, *Phys. Rev. Lett.* **111**, 237405(2013).
 - [12] Ermin Malic, Torben Winzer, Evgeny Bobkin, and Andreas Knorr, *Phys. Rev. B* **84**, 205406(2011).
 - [13] Han Hsu and L. E. Reichl, *Phys. Rev. B* **76**, 045418(2007).
 - [14] Xiao-Liang Qi and Shou-Cheng Zhang, *Rev. Mod. Phys.* **83**, 1057(2011).